A Letters Journal Exploring the Frontiers of Physics

December 2019

EPL, **128** (2019) 58003 www.epljournal.org
doi: 10.1209/0295-5075/128/58003

Aging transition under weighted conjugate coupling

K. Ponrasu[1], I. Gowthaman[1] V. K. Chandrasekar[1(a)] and D. V. Senthilkumar[2(b)]

[1] *Centre for Nonlinear Science & Engineering, School of Electrical & Electronics Engineering, SASTRA Deemed University - Thanjavur-613 401, Tamil Nadu, India*
[2] *School of Physics, Indian Institute of Science Education and Research - Thiruvananthapuram-695 551, Kerala, India*

received 9 September 2019; accepted in final form 20 December 2019
published online 4 February 2020

PACS 89.75.-k – Complex systems
PACS 89.75.Fb – Structures and organization in complex systems
PACS 05.45.Xt – Synchronization; coupled oscillators

Abstract – We investigate the effect of symmetry breaking couplings on the macroscopic dynamical behavior of an ensemble of globally coupled active and inactive oscillators. Conjugate coupling among the ensemble and the weighted coupling within the active and inactive groups introduces the asymmetry. Large values of the global coupling strength facilitate the onset of the phenomenon of aging transition, thereby deteriorating the macroscopic oscillatory behavior. We find that the natural frequency of oscillation favors the onset of the aging transition even in the presence of a large proportion of the active oscillators because of the broken symmetry. Further the ratio of the intra-group (weighted) couplings plays a nontrivial role in determining the dynamical behaviors and their transitions. It is also observed that even a feeble change in the simple feedback factor in the coupling facilitates the counterintuitive effect of preserving the macroscopic oscillatory nature of the ensemble, comprising completely inactive oscillators, in the entire parameter space where the ensemble suffered the aging transition.

Introduction. – The framework of coupled oscillators serves as an excellent platform to unravel a plethora of macroscopic dynamical behaviors, including the intriguing role of their microscopic constituents, such as pattern formation, clustering, synchronization, quenching of oscillations, chimera states, etc. [1–11], mimicking several real world phenomena. Further, such a framework facilitates the rigorous analytical treatment of several macroscopic phenomena even in the thermodynamic limit [12,13]. Deterioration of dynamical units at the microscopic level of a large collection of oscillators severely affects the macroscopic properties of the network as a whole. For instance, a common cause for several neuronal disorders including Alzheimer's disease is the failure of neurons in assemblies despite the fact that billions of neurons are born and die every day. In relation to this, a phenomenon termed "aging transition" was reported by Daido and Nakanishi [14] by increasing the proportion of inactive oscillators in an ensemble of globally coupled active and inactive oscillators. Later, this phenomenon was even extended to an ensemble of heterogeneous oscillators [15] along with different coupling configurations [16,17].

Recent renewed bursts of activity regarding the aging transition (AT) have been dealing with preventing the onset of the AT by adopting various control mechanisms to retain the macroscopic properties of the ensemble of oscillators. In particular, recent publications on the phenomenon of reviving of oscillations [18,19], which essentially refers to the restoration of oscillations of a coupled network from their stable homogeneous/inhomogeneous steady states, has seeded the momentum. Specifically, a simple limiting feedback factor in the standard diffusive coupling was introduced to sustain the macroscopic behavior thereby preventing the onset of the AT [20], random errors (uniform and normal) in the distance parameters were shown to persist the macroscopic dynamical activity [21], employing auxiliary oscillators was also shown to prevent the onset of the AT [22], and an asymmetry coupling between the two populations has been introduced recently to elucidate the enhanced robustness of the collection of active and inactive oscillators [23].

In this letter, we employ the conjugate coupling among the globally coupled oscillators comprising active and

(a) E-mail: chandru25nld@gmail.com (corresponding author)
(b) E-mail: skumar@iisertvm.ac.in (corresponding author)

inactive ones, so that the conjugate coupling [24–27] introduces asymmetry by breaking the rotational symmetry of the globally coupled oscillators with standard diffusive coupling. Further, we introduce an additional asymmetry between the active and inactive group of oscillators by employing weighted coupling so that the two groups of oscillators interact with different coupling strengths. Our main aim is to investigate the interplay of the conjugate coupling and the asymmetry parameter, along with the natural frequency of the oscillators facilitating the onset of the *AT*. We find that the *AT* occurs even in the presence of an appreciable number of active oscillators upon increasing the coupling strength beyond the unit value. Increasing the natural frequency of the oscillators decreases the critical value of the ratio of the inactive oscillators, for a given coupling strength, at which the *AT* occurs.

The interplay of the asymmetry parameter, which weights the influence of one group on the other, plays a crucial role in determining the onset of the *AT*. The macroscopic oscillatory (homogeneous steady) state is favoured when the influence of the active (inactive) oscillators is stronger than that of their counterparts. Further, the transition from limit-cycle oscillations (*LC*) to the stable homogeneous steady state (*HSS*), corresponding to *AT*, occurs via an inverse Hopf bifurcation, while the transition from stable inhomogeneous steady state (*IHSS*) to the *AT* onsets via a pitch-fork bifurcation. The onset of *IHSS*, that is the oscillation death state has already been reported using the conjugate coupling under different contexts/conditions [24–27]. The transition from oscillatory to *IHSS* is favored through a saddle-node bifurcation. Hopf and pitch-fork bifurcation curves are deduced analytically using the linear stability analysis and the Routh-Hurwitz criterion. We have also introduced a limiting factor in the conjugate coupling to unravel its role in increasing the robustness of the macroscopic oscillatory nature of the network. We find that even a small decrease in the value of the limiting factor increases the parameter space of macroscopic oscillations to a large extent. Below a critical value the homogeneous steady state constituting the *AT* region disappears completely from the entire parameter space thereby retaining the macroscopic oscillations, and hence increasing their robustness, surprisingly even in an ensemble comprised only of inactive oscillators.

The model. – We consider the paradigmatic model of globally coupled Stuart-Landau limit-cycle oscillators with conjugate coupling, whose governing equation of motion can be represented as

$$\begin{aligned}\dot{z}_j &= (\lambda_j + i\omega - |z_j|^2)z_j + \frac{m_{(1,2)}\varepsilon}{N}\sum_{k=1}^{N}[(\mathrm{Im}(z_k) \\ &\quad - \alpha\mathrm{Re}(z_j)) + i(\mathrm{Re}(z_k) - \alpha\mathrm{Im}(z_j))], \end{aligned} \tag{1}$$

where the state variable $z_j = x_j + iy_j \in C$, $j = 1, \ldots, N$, x_j and y_j are the real variables and N is the total number of oscillators. ω is the natural frequency of the oscillators, ε is the coupling strength, α is the feedback control parameter which ranges from $0 \leq \alpha \leq 1$. When $\alpha = 0$, the coupling in (1) is a direct coupling, whereas it is a standard global diffusive coupling for $\alpha = 1$. The globally coupled oscillators consist of active oscillators exhibiting limit-cycle oscillations for $\lambda_j = 2$ and inactive oscillators with stable homogeneous steady state for $\lambda_j = -1$. Specifically the value of λ in the Stuart-Landau limit-cycle oscillator attributes to the fact that whether the limit-cycle oscillation emerges through a supercritical ($\lambda_j > 0$) or a subcritical ($\lambda_j < 0$) Hopf bifurcation. It is to be noted that the Stuart-Landau oscillator represents the normal form of the Hopf bifurcation and hence a large class of nonlinear oscillators near the Hopf bifurcation can be approximated as the Stuart-Landau limit-cycle oscillator. The oscillators $N_1 = j \in (1, \ldots, N(1-p))$ correspond to the active oscillators, while the remaining $N_2 = j \in (N(1-p)+1, \ldots, N)$ oscillators are inactive, such that $N = N_1 + N_2$. p quantifies the ratio of the inactive oscillators. All the N oscillators are active for $p = 0$, while they are all inactive for $p = 1$. The intra-groups of active and inactive oscillators will have their coupling strengths m_1 and m_2, respectively. An asymmetric interaction similar to that in eq. (1) using the parameters m_1 and m_2 occurs in wide natural systems such as prey-predator systems, neural populations, community structures, hierarchical networks and so on. However, it predominantly occurs in ecological systems, for instance the asymmetry interaction corresponds to the dispersal rate in metapopulations [28]. In the present context, the asymmetry interaction was already shown to augment the dynamical persistence among the population of active and inactive oscillators [23].

Stability analysis: Hopf and pitch-fork bifurcation curves. – The two groups of active (A) and inactive (I) oscillators collapse to a single group of inactive oscillators, resulting in a global homogeneous steady state, at the critical value of the fraction of the inactive oscillators p_c, at which the *AT* occurs. Since $A = A_r + iA_{im}$ and $I = I_r + iI_{im}$, where A_r, A_{im}, I_r and I_{im} are the real variables, the evolution equation in terms of their real variables can be represented as

$$\begin{aligned}\dot{A}_r &= aA_r - A_{im}\omega - A_rA_{im}^2 - A_r^3 + m_1\varepsilon[(1-p)A_{im} \\ &\quad + pI_{im} - \alpha A_r], \end{aligned} \tag{2a}$$

$$\begin{aligned}\dot{A}_{im} &= aA_{im} + A_r\omega - A_{im}A_r^2 - A_{im}^3 + m_1\varepsilon[(1-p)A_r \\ &\quad + pI_r - \alpha A_{im}], \\ \dot{I}_r &= bI_r - I_{im}\omega - I_rI_{im}^2 - I_r^3 + m_2\varepsilon[(1-p)A_{im} \\ &\quad + pI_{im} - \alpha I_r], \end{aligned} \tag{2b}$$

$$\begin{aligned}\dot{I}_{im} &= bI_{im} + I_r\omega - I_{im}{I_r}^2 - I_{im}^3 + m_2\varepsilon[(1-p)A_r \\ &\quad + pI_r - \alpha I_{im}], \end{aligned}$$

where $a = 2$ and $b = -1$. One can obtain the critical value of p by the linear stability analysis of the above equations at the origin $(A, I) = (0, 0)$. The characteristic equation deduced from the Jacobian of the above system

of equations can be represented as

$$\lambda^4 + c_1\lambda^3 + c_2\lambda^2 + c_3\lambda^1 + c_4\lambda^0 = 0, \quad (3)$$

where the coefficients c_i can be deduced as

$$\begin{aligned}
c_1 &= 2b - 2a + 2\varepsilon m_1\alpha + 2\varepsilon m_2\alpha,\\
c_2 &= a^2 + b^2 - \varepsilon^2 m_1^2 + 2\varepsilon^2 m_1^2 p - 2\varepsilon^2 m_1 m_2 p - \varepsilon^2 m_1^2 p^2\\
&\quad + 2\varepsilon^2 m_1 m_2 p^2 - \varepsilon^2 m_2^2 p^2 + 2b\varepsilon(2m_1 + m_2)\alpha\\
&\quad + \varepsilon^2 m_1^2\alpha^2 + 4\varepsilon^2 m_1 m_2\alpha^2 + \varepsilon^2 m_2^2\alpha^2\\
&\quad - 2a(2b + \varepsilon(m_1 + 2m_2)\alpha) + 2\omega^2,\\
c_3 &= 2(b^2\varepsilon m_1\alpha + a^2(b + \varepsilon m_2\alpha) - a(b^2 + 2b\varepsilon(m_1 + m_2)\alpha\\
&\quad + \varepsilon^2 m_2(m_2(\alpha^2 - p^2) + m_1(p^2 + 2\alpha^2 - p)) + \omega^2)\\
&\quad + b(\varepsilon^2 m_1(m_1(2p - 1 - p^2 + \alpha^2)\\
&\quad + m_2(p^2 - p + 2\alpha^2)) + \omega^2) + \varepsilon\alpha(\varepsilon^2 m_1 m_2(m_2(\alpha^2 - p)\\
&\quad + m_1(p - 1 + \alpha^2)) + (m_1 + m_3)\omega^2)),\\
c_4 &= \varepsilon^4 m_1^2 m_2^2\alpha^4 - \varepsilon^4 m_1^2 m_2^2\alpha^2 - \varepsilon^2 m_1^2\omega^2 + 2\varepsilon^2 m_1^2 p\omega^2\\
&\quad - 2\varepsilon^2 m_1 m_2 p\omega^2 - \varepsilon^2 m_1^2 p^2\omega^2 + 2\varepsilon^2 m_1 m_2 p^2\omega^2\\
&\quad - \varepsilon^2 m_2^2 p^2\omega^2 + \varepsilon^2 m_1^2\alpha^2\omega^2 + \varepsilon^2 m_2^2\alpha^2\omega^2 + \omega^4\\
&\quad + b^2(\varepsilon^2 m_1^2(2p - 1 - p^2 + \alpha^2) + \omega^2) + 2b\varepsilon m_2\alpha\\
&\quad (\varepsilon^2 m_1^2(p - 1 + \alpha^2) + \omega^2) + a^2(b^2 + 2b\varepsilon m_2\alpha\\
&\quad + \varepsilon^2 m_2^2(\alpha^2 - p^2) + \omega^2) - 2a\varepsilon m1(b^2\alpha\\
&\quad + b\varepsilon m_2(p^2 - p + 2\alpha^2) + \alpha(\varepsilon^2 m_2^2(\alpha^2 - p) + \omega^2)).
\end{aligned}$$

However, solving the fourth-order characteristic equation to deduce the critical curves, across which the bifurcation occurs, from the eigenvalue analysis is a difficult task. Nevertheless, one can arrive at the Hopf and pitch-fork bifurcation points/curves using the coefficients of the characteristic equation following the Routh-Hurwitz stability criterion [29]. All the other conditions are satisfied automatically for the chosen parameters except for

$$f(\varepsilon, \alpha, m_1, m_2, p) = c_1c_2c_3 - (c_3^2 + c_1^2c_4) > 0, \quad (4)$$

and $c_4 > 0$. One can deduce the critical value of the fraction of inactive oscillators corresponding to the AT, onsets via the Hopf bifurcation, by solving the function $f(\varepsilon, \alpha, m_1, m_2, p_{HB}) = 0$, which results in the Hopf bifurcation curve. Upon equating $c_4 = 0$, one can deduce the pitch-fork bifurcation curve as

$$\begin{aligned}
p_{PB} &= \frac{1}{S}\left[\varepsilon^2 m_1^2(b^2 + \omega^2) + \varepsilon^2 m_1 m_2(ab - \omega^2)\right]\\
&\quad + \alpha\varepsilon^3(bm_1m_2 + am_1m_2^2) - \sqrt{\Delta}, \quad (5)
\end{aligned}$$

where

$$\begin{aligned}
\Delta &= G_1 + G_2,\\
G_1 &= \varepsilon^4 m_1^2[b^2m_1 + a\varepsilon m_2^2\alpha + bm_2(a + \varepsilon m_1\alpha)\\
&\quad + (m_1 - m_2)\omega^2]^2,\\
G_2 &= (b^2 + 2b\varepsilon m_2\alpha + \varepsilon^2 m_2^2\alpha^2 + \omega^2)(a^2 + 2a\varepsilon m_1\alpha\\
&\quad + k^2 m_1^2(\alpha^2 - 1) + \omega^2)S,\\
S &= \varepsilon^2[b^2m_1^2 + 2abm_1m_2 + a^2m_2^2 + (m_1 - m_2)^2\omega^2].
\end{aligned}$$

Dynamical transitions. – In order to discuss the dynamical transitions more elaborately, we numerically solve the above system of eqs. (1) using the Runge-Kutta fourth-order integration scheme with a step size of 0.01. Particularly, we estimate the normalized order parameter $R \equiv |Z(p)|/|Z(0)|$ of the coupled systems, where $Z = \frac{1}{N}\sum_{j=1}^{N} z_j$. We have fixed the number of oscillators in the ensemble as $N = 500$ throughout the paper. The normalized order parameter R as a function of the ratio of inactive oscillators p is depicted in fig. 1 for three different coupling strengths. The natural frequencies of the oscillators are fixed as $\omega = 1.0$ and 2.0 in fig. 1(a) and 1(b), respectively, while the asymmetry parameters corresponding to the weighted coupling (intra-group coupling strength) are chosen as $m_1 = m_2 = 1$. It is evident from fig. 1(a) that the oscillators in the ensemble gradually reach the *HSS* in proportion to the number of inactive oscillators p, as indicated by the declining value of the order parameter, and eventually all the oscillators destined to the *HSS* at $p = 1$ for $\varepsilon = 1$. Thus the macroscopic oscillatory nature of the ensemble is lost completely by choice, only when all the oscillators constituting the ensemble are chosen to be inactive, to get entrained to the stable HSS for the unit value of the coupling strength. In contrast, the ensemble of globally coupled oscillators display the AT even at finite proportion of the inactive oscillators p less than unity for large values of ε. For instance, the AT occurs at $p = 0.78$ and 0.77 for $\varepsilon = 3$ and 5 (see fig. 1(a)), respectively, where there exists an appreciable number of active oscillators in the ensemble.

Further, the effect of increasing the natural frequency of oscillators to $\omega = 2$ can be appreciated from fig. 1(b). For $\varepsilon = 1$, the ensemble undergoes a synchronization transition to *HSS* when all the oscillators in the ensemble are inactive. On the other hand, it is interesting to witness that the ensemble suffers the AT even at very low values of p upon increasing the natural frequency of the oscillators in the ensemble. For instance, the AT occurs even at $p = 0.45$ and 0.64 for $\varepsilon = 3$ and 5, respectively, for $\omega = 2$ (see fig. 1(b)). These results elucidate that the AT occurs even at low values of the critical ratio of the inactive oscillators p_c despite the presence of a large proportion of the active oscillators, for a given coupling strength, upon increasing the frequency of the oscillators. It is to be noted that the frequency-dependent AT occurs due to the conjugate coupling, which breaks the rotational symmetry of the globally coupled oscillators in contrast to the existing reports on the AT. Further, it is also clear that the AT occurs at low values of p upon increasing the coupling strength for a fixed frequency of the oscillators.

Now, we will unravel the influence of the asymmetry parameters (intra-group coupling strengths) m_1 and m_2 on the phenomenon of the AT. The order parameter as a function p is depicted in fig. 2 for three different coupling strengths. First, we fix the intra-group coupling strength of the active oscillators as $m_1 = 1$ and vary that of the

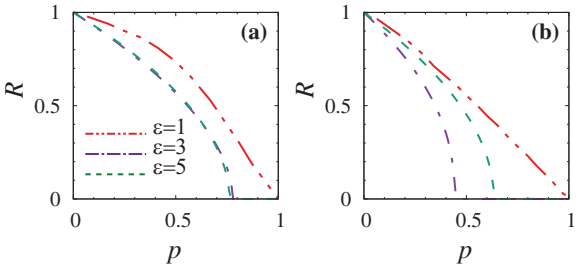

Fig. 1: The normalized order parameter R as a function of the ratio of the inactive oscillators p. (a) $\omega = 1.0$ and (b) $\omega = 2.0$. The other parameters are $a = 2.0$, $b = -1.0$, $\alpha = 1.0$, and $m_1 = m_2 = 1.0$.

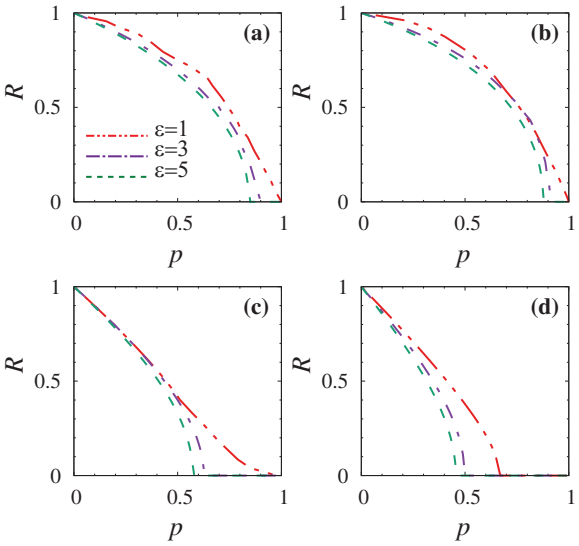

Fig. 2: The normalized order parameter R as a function of the ratio of the inactive oscillators p for $\omega = 1.0$. (a) $m_1 = 1, m_2 = 2$, (b) $m_1 = 1, m_2 = 3$, (c) $m_1 = 2, m_2 = 1$, and (d) $m_1 = 3, m_2 = 1$. The other parameters are the same as in fig. 1.

inactive oscillators as $m_2 = 2$ and 3 in figs. 2(a) and 2(b), respectively. Since the oscillators are globally coupled, the influence of the active (inactive) group will be stronger than that of the inactive (active) group for larger values of m_2 (m_1). Hence, the ensemble of active and inactive oscillators exhibit the AT at increasingly higher values of p for decreasing values of the coupling strength ε for $m_2 = 2$ (see fig. 2(a)). The AT occurs at further larger values of p for the corresponding ε for further increase in m_2 as depicted in fig. 2(b) for $m_2 = 3$ as the influence of the active oscillators become much stronger than that of the inactive oscillators. By fixing the intra-group coupling strength of the inactive oscillators as $m_2 = 1$, now we will investigate the influence of m_1. The AT of the globally coupled Stuart-Landau oscillators is shown in figs. 2(c) and 2(d), respectively, for $m_1 = 2$ and 3. As the influence of the inactive oscillators on the active oscillators becomes stronger for increasing values of m_1, the AT occurs even

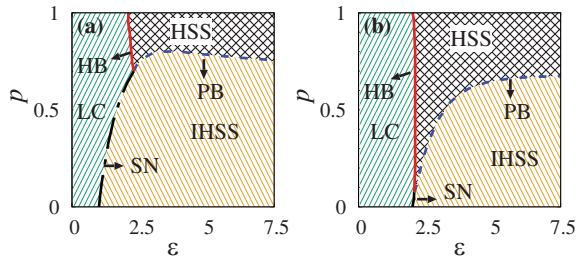

Fig. 3: Two-parameter phase diagrams in the (ε, p) space for the natural frequency of the oscillators (a) $\omega = 1$, and (b) $\omega = 2$. The other parameters are the same as in fig. 1. *HSS* corresponds to the aging transition, *IHSS* to the oscillation death state and *LC* refers to the limit-cycle oscillations. *HB*, *PB* and *SN* correspond to the Hopf, pitch-fork and saddle-node bifurcations, respectively.

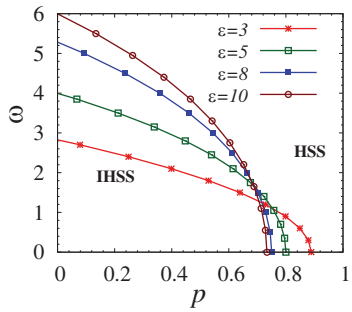

Fig. 4: Two-parameter space as a function of the proportion of inactive oscillators p and the natural frequency ω. Lines connected by different symbols correspond to the pitch-fork bifurcation curve demarcating the homogeneous (AT) and inhomogeneous steady states for different values of the coupling strength.

for low values of p as a function of m_1 and ε despite the presence of a large proportion of the active oscillators.

The global dynamical transition as a function of ε and p is depicted as two-parameter phase diagrams in fig. 3 for two different frequency of oscillations corresponding to fig. 1. The other parameters are also the same as in fig. 1. Comparing figs. 3(a) and 3(b), the spread of the AT region increases to a large extent for $\omega = 2$ (see fig. 3(b)). There lies a minimum value of ε above which the AT occurs as a function of p. However, all the oscillators will be inactive, corresponding to the synchronized *HSS*, in the entire range of ε for $p = 1$. It is to be noted that the pitch-fork bifurcation curve in fig. 3(b), across which AT onsets, emerges nearly from $p = 0$ and $\varepsilon = 2.3$. As the coupling strength is increased, the critical values of ε and p corresponding to the pitch-fork bifurcation curve increase and then saturate as a function of ε elucidating that for low values of ε AT occurs earlier than for high values of ε. It is also evident from fig. 4 as a function of p and ω for different ε. It is to be noted that for lower values of ω (for $\omega < 1.3$) AT occurs for higher values of ε, whereas for $\omega \geq 1.3$ AT occurs for lower values of ε first and then at

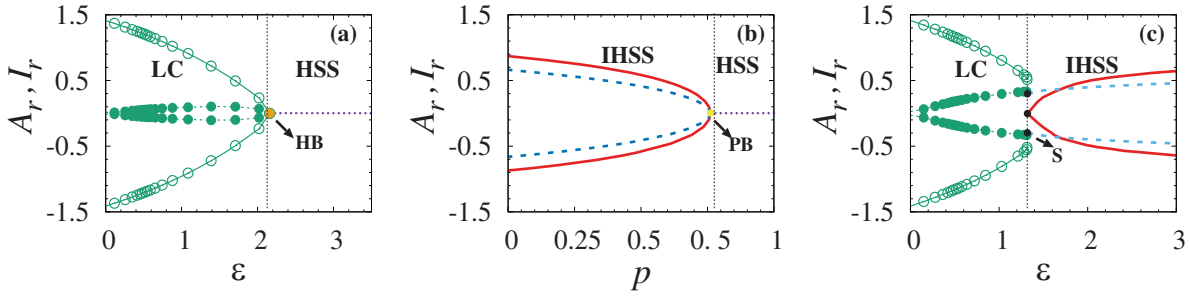

Fig. 5: Bifurcation diagrams using XPPAUT for the system (2) for $\omega = 1.0$ and for (a) $p = 0.8$, (b) $\varepsilon = 5$, and (c) $p = 0.3$. See text for details.

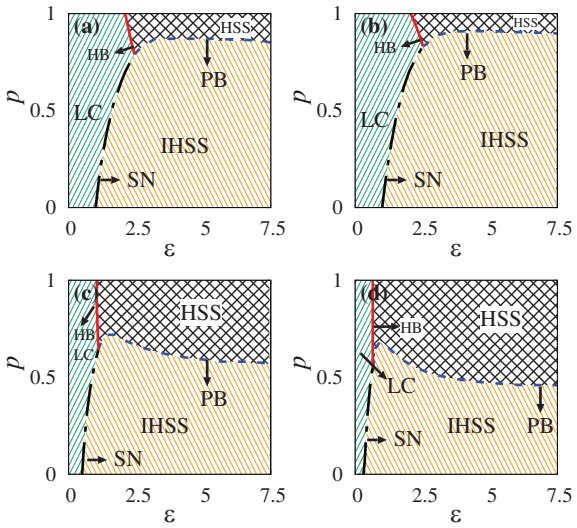

Fig. 6: Two-parameter plot in the (ε, p) space for $\omega = 1$. (a) $m_1 = 1, m_2 = 2$, (b) $m_1 = 1, m_2 = 3$, (c) $m_1 = 2, m_2 = 1$, and (d) $m_1 = 3, m_2 = 1$. The other parameters are the same as in fig. 1.

higher values. Further, it is also evident from the figure that a large frequency of oscillation favors the onset of aging transition even in the absence of inactive oscillators. Three different bifurcations responsible for the dynamical transitions observed in fig. 3 are depicted in fig. 5.

One-parameter bifurcation diagrams of both active and inactive group of oscillators obtained using the software XPPAUT [30] are depicted in fig. 5. Solid (dashed) lines correspond to stable *IHSS* of active (inactive) oscillators. *HSS* (*AT*) is indicated by the dotted line. Lines connected by open (filled) circles correspond to the dynamics of active (inactive) limit-cycle oscillators. *SN*, *HB* and *PB* represent saddle-node, Hopf and pitch-fork bifurcations. There is transition from *LC* to *HSS* (*AT*) via a Hopf bifurcation as a function of ε as depicted in fig. 5(a) for $p = 0.8$. The transition from the *IHSS* state to the *HSS* occurs via a pitch-fork bifurcation as a function of p (see fig. 5(b) for $\varepsilon = 5$). A saddle-node bifurcation mediates the transition from *LC* to *IHSS* as a function of ε as shown in fig. 5(c) for $p = 0.3$. The Hopf and pitch-fork bifurcation curves, represented by solid and dashed lines, respectively, in fig. 3 delineating the boundaries between different dynamical states are the analytical bifurcation curves, whereas the saddle-node bifurcation curve, represented by a dash-dotted line, was obtained from the XPPAUT.

The two-parameter phase diagram in the (ε, p) space corresponding to dynamical transitions in fig. 2 is depicted in fig. 6. Since the influence of the active oscillators is stronger for larger values of m_2 for a fixed m_1, the spread of the *HSS* (*AT* region) decreases as a function of p and ε from figs. 3(a) to 6(b) via fig. 6(a) for increasing values of m_2. Similarly to fig. 3, there is an *AT* from oscillatory state via a Hopf bifurcation. Further, there is a transition from *IHSS* to *HSS* via a pitch-fork bifurcation and the transition from oscillatory to *OD* state is mediated by a saddle-node bifurcation. Figures 6(c) and 6(d) are plotted for $m_1 = 2$ and 3, respectively, for a fixed $m_2 = 1$. It is evident that the spread of the *AT* region increases for increasing m_1 as the influence of the inactive oscillators is stronger than that of the active oscillators. Further, all the oscillators are in the stable synchronized *HSS* for $p = 1$ irrespective of the value of ε, m_1, m_2 and ω.

The two-parameter phase diagram as a function of the coupling strength ε and the frequency of oscillation ω is shown in fig. 7 for $p = 0.8$. Essentially, the dynamical transitions occur through the three bifurcations, as in figs. 3 and 6, which are depicted in fig. 7(a) for $m_1 = m_2 = 1$. The spread of the *AT* increases both as a function of the natural frequency of oscillators and the coupling strength ε. Upon increasing the coupling strength of inactive oscillators to $m_2 = 2$, the spread of the *AT* region decreases both as a function of ω and ε, as illustrated in fig. 7(b), as the influence of the active oscillators will be stronger than that of the inactive group of oscillators. In contrast, the spread of the *AT* region increases upon increasing the coupling strength of the active oscillators to $m_1 = 2$ (see fig. 7(c)) as the influence of inactive oscillators is much stronger than that of the active oscillators in the ensemble of globally coupled Stuart-Landau oscillators with conjugate coupling. Further, the spread of the *HSS* in the two-parameter (ε, ω) space for different combinations of m_1 and m_2 is depicted in fig. 8 for $p = 0.8$. The dynamical

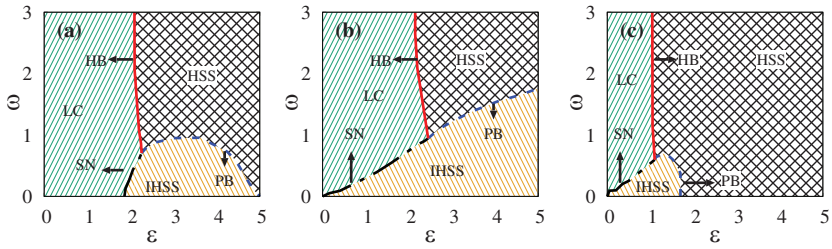

Fig. 7: Two-parameter plot in the (ε, ω) space for $p = 0.8$. (a) $m_1 = m_2 = 1$, (b) $m_1 = 1, m_2 = 2$ and (c) $m_1 = 2, m_2 = 1$. The other parameters are the same as in fig. 1.

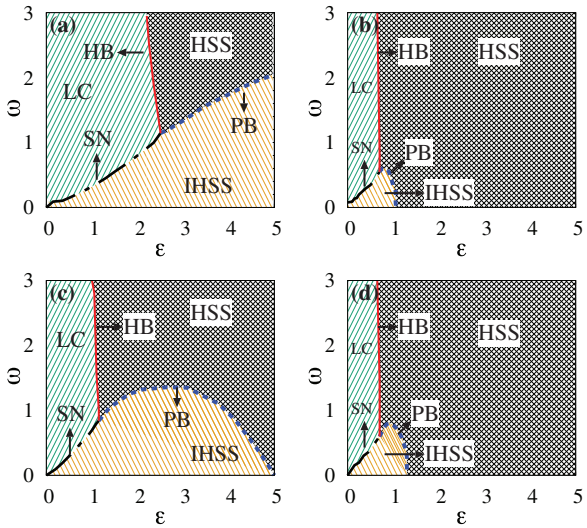

Fig. 8: Two-parameter plot in the (ε, ω) space for $p = 0.8$. (a) $m_1 = 1, m_2 = 3$, (b) $m_1 = 3, m_2 = 1$, (c) $m_1 = 2, m_2 = 3$ and (d) $m_1 = 3, m_2 = 2$. The other parameters are the same as in fig. 1.

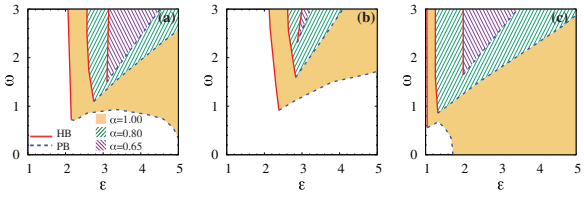

Fig. 9: Aging islands for different values of α in the (ε, ω) space for $p = 0.8$. The other parameters are the same as in fig. 1. (a) $m_1 = m_2 = 1$, (b) $m_1 = 1, m_2 = 2$ and (c) $m_1 = 2$, $m_2 = 1$.

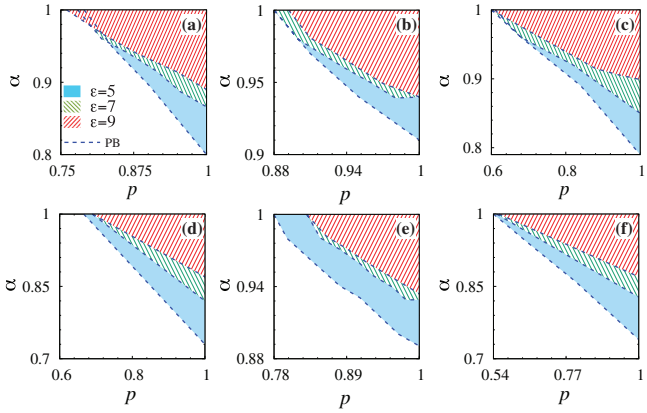

Fig. 10: Aging islands in the (p, α) parameter space for different ε. Top row: $\omega = 1$. Bottom row: $\omega = 2$. The other parameters are the same as in fig. 1. (a) $m_1 = m_2 = 1$, (b) $m_1 = 1, m_2 = 2$, (c) $m_1 = 2, m_2 = 1$, (d) $m_1 = m_2 = 1$, (e) $m_1 = 1, m_2 = 2$, and (f) $m_1 = 2, m_2 = 1$.

transitions along with the nature of bifurcations are similar to fig. 7 except for the difference in the spread of the dynamical states. For $m_1 = 1$ and $m_2 = 3$, the influence of the active oscillators is stronger than that of the inactive oscillators and hence spread of the AT region is rather low in the (ε, ω) space in fig. 8(a), whereas the spread of the AT region is large for larger values of m_1 as can be seen in fig. 8(b) for $m_1 = 3$ and $m_2 = 1$, in which case the influence of the inactive oscillators is stronger. Figures 8(c) and 8(d) are plotted for $(m_1 = 2, m_2 = 3)$ and $(m_1 = 3, m_2 = 2)$, respectively, which indeed corroborates the influence of active and inactive oscillators in line with the above results.

The critical curves (Hopf and pitch-fork bifurcation curves) enclosing the AT (shaded) region for different values of the feedback factor are shown in fig. 9. The spread of the AT region in the (ε, ω) space is depicted in fig. 9(a) for $m_1 = m_2 = 1$ for three different α. It is evident from the figure that the spread of the AT region decreases upon decreasing the feedback parameter and finally below a critical value the AT region disappears completely thereby resulting only in the macroscopic oscillatory state in the entire parameter space. Similar results are also observed in fig. 9(b) and fig. 9(c) for $(m_1 = 1, m_2 = 2)$ and $(m_1 = 2, m_2 = 1)$, respectively.

Now, the spread of the AT region enclosed by the pitch-fork bifurcation curve in the (p, α) space for different values of the coupling strength is shown in fig. 10. The top row in fig. 10 is plotted for $\omega = 1$, while the bottom row is depicted for $\omega = 2$. Figures 10(a) and 10(d) are depicted for $m_1 = m_2 = 1$. It is evident from these figures that the spread of the AT decreases upon decreasing values

of the feedback parameter α and below a critical value, it surprisingly disappears even for $p = 1$. Astoundingly, even the entire group of inactive oscillators starts oscillating below a critical value of α. Further, the spread of the AT region is depicted in figs. 10(b) and 10(e) for $m_1 = 1$ and $m_1 = 2$, while in figs. 10(c) and 10(f) for $m_1 = 2$ and $m_1 = 1$. All these figures confirm that below a critical value of the feedback parameter α the AT region disappears thereby reviving the oscillations back in the same parameter space where the ensemble of globally coupled identical Stuart-Landau oscillators underwent the stable *HSS* (AT).

Conclusions. – We have considered globally coupled active and inactive oscillators with weighted coupling to investigate the aging transition. To the best of our knowledge, it is the first report on the AT employing symmetry breaking conjugate coupling. For lower values of ω, AT occurs as a function of ε, however for higher ω, AT occurs at lower values of ε first and then at higher ε. Further, it is also evident that a large frequency of oscillation favors the onset of aging transition even in the absence of inactive oscillators. Increasing ω and ε is found to facilitate the onset of the aging transition even at low values of p, where there exists a large proportion of active oscillators. Further, we have also shown that increasing the intra-group coupling strength of active (inactive) oscillators enhances the spread of the aging transition (oscillatory) region as their counterparts will have stronger influence over the other. In particular, we have extensively investigated the effect of asymmetric interaction among the active and inactive oscillators. Further, we have also confirmed that our results are robust in a large range of λ for active and inactive populations and ω. Astoundingly, even a feeble decrease in the limiting factor α in the coupling retrieves the macroscopic oscillatory nature of the network even for $p = 1$, thereby enhancing the robustness of the macroscopic dynamical behavior.

* * *

KP and IG wish to thank SASTRA Deemed University for research fund and extending infrastructure support to carry out this work. DVS is supported by the CSIR EMR Grant No. 03(1400)/17/EMR-II. The work of VKC is part of a research project sponsored by CSIR Project under Grant No. 03(1444)/18/EMR-II.

REFERENCES

[1] Strogatz S. H., *Sync: How Order Emerges from Chaos in the Universe, Nature and Daily Life* (Hyperion, New York) 2012.
[2] Kuramoto Y., *Chemical Oscillations, Waves, and Turbulence* (Springer, Berlin) 1984.
[3] Pikovsky A. S., Rosenblum M. G. and Kurths J., *Synchronization. A Universal Concept in Nonlinear Sciences* (Cambridge University Press, Cambridge) 2001.
[4] Boccaletti S., Kurths J., Osipov G., Valladares D. L. and Zhou C. S., *Phys. Rep.*, **366** (2002) 1.
[5] Boccaletti S., Latora V., Moreno Y., Chavez M. and Hwang D.-U., *Phys. Rep.*, **424** (2006) 175.
[6] Arenas A., Díaz-Guilera A., Kurths J., Moreno Y. and Zhou C. S., *Phys. Rep.*, **469** (2008) 93.
[7] Lakshmanan M. and Senthilkumar D. V., *Dynamics of Nonlinear Time-Delay Systems* (Springer, Berlin, Heidelberg) 2011.
[8] Nan Yao and Zheng Z., *Int. J. Mod. Phys. B*, **30** (2016) 1630002.
[9] Schöll E., *Eur. Phys. J. ST*, **225** (2016) 891.
[10] Saxena G., Prasad A. and Ramaswamy R., *Phys. Rep.*, **521** (2012) 205.
[11] Koseska A., Volkov E. and Kurths J., *Phys. Rep.*, **531** (2013) 173.
[12] Ott E. and Antonsen T. M., *Chaos*, **18** (2008) 037113; **19** (2009) 023117.
[13] Abrams D. M. and Strogatz S. H., *Phys. Rev. Lett.*, **77** (1996) 1406.
[14] Daido H. and Nakanishi K., *Phys. Rev. Lett.*, **93** (2004) 104101; *Phys. Rev. E*, **75** (2007) 056206.
[15] Gouhei Tanaka, Kai Morino, Hiroaki Daido and Kazuyuki Aihara, *Phys. Rev. E*, **89** (2014) 052906.
[16] Daido H., *EPL*, **84** (2008) 10002; **87** (2009) 40001; *Phys. Rev. E*, **83** (2011) 026209; **87** (2011) 016215.
[17] Morino K., Tanaka G. and Aihara K., *Phys. Rev. E*, **83** (2011) 056208.
[18] Zou W., Senthilkumar D. V., Zhan M. and Kurths J., *Phys. Rev. Lett.*, **111** (2013) 014101.
[19] Zou W., Senthilkumar D. V., Nagao R., Kiss I. Z., Tang Y., Koseska A., Duan J. and Kurths J., *Nat. Commun.*, **6** (2015) 7709.
[20] Liu Y., Zou W., Zhan M., Duan J. and Kurths J., *EPL*, **114** (2016) 40004.
[21] Sun Z., Ma N. and Xu W., *Sci. Rep.*, **7** (2017) 42715.
[22] Morino K., Tanaka G. and Aihara K., *Phys. Rev. E*, **88** (2013) 032909.
[23] Kundu S., Majhi S., Karmakar P., Ghosh D. and Rakshit B., *EPL*, **123** (2018) 30001.
[24] Punetha Nirmal, Varshney Vaibhav, Sahoo Samir, Saxena Garima, Prasad Awadhesh and Ramaswamy Ram, *Phys. Rev. E*, **98** (2018) 022212.
[25] Nannan Zhao, Zhongkui Sun and Wei Xu, *Sci. Rep.*, **8** (2018) 8721.
[26] Wenchen Han, Hongyan Cheng, Qionglin Dai, Haihong Li, Ping Ju and Junzhong Yang, *Commun. Nonlinear Sci. Numer. Simul.*, **39** (2016) 73.
[27] Nannan Zhao, Zhongkui Sun, Xiaoli Yang and Wei Xu, *Phys. Rev. E*, **97** (2018) 062203.
[28] Kundu S., Majhi S., Sourav K. S., Ghosh D. and Rakshit B., *Phys. Rev. E*, **96** (2017) 062212.
[29] Liu W. M. and Math J., *Anal. Appl.*, **182** (1994) 250.
[30] Ermentrout B., *Simulating, Analyzing and Animating Dynamical Systems: A Guide to Xppaut for Researchers and Students (Software, Environments, Tools)* (SIAM Press, Philadelphia, Penn.) 2002.